Zhang and Wang *Satellite Navigation* (2023) 4:10
https://doi.org/10.1186/s43020-023-00099-1

Satellite Navigation
https://satellite-navigation.springeropen.com/

ORIGINAL ARTICLE Open Access

Integrity monitoring scheme for single-epoch GNSS PPP-RTK positioning

Wenhao Zhang* and Jinling Wang

Abstract

Integrity monitoring for precise point positioning is critical for safety-related applications. With the increasing demands of high-accuracy autonomous navigation for unmanned ground and aerial vehicles, the integrity monitoring method of high-precision positioning has become an essential requirement. While high precision Global Navigation Satellite Systems (GNSS) positioning is widely used in such applications, there are still many difficulties in the integrity monitoring method for the multi-frequency multi-GNSS undifferenced and uncombined Precise Point Positioning (PPP). The main difficulties are caused by using the measurements of multiple epochs in PPP. Based on the baseline Multiple Hypothesis Solution Separation (MHSS) Advanced Receiver Autonomous Integrity Monitoring (ARAIM) algorithm, this paper discusses the feasibility of the pseudorange-based baseline ARAIM method on the single-epoch PPP based on Real-Time Kinematic (RTK) networks (PPP-RTK) framework to overcome these difficulties. In addition, a new scheme is proposed to transfer the conventional PPP process into the single-epoch PPP-RTK framework. The simulation results using the proposed model are analyzed in this study. The Protection Levels (PLs) estimated by PPP Wide-lane Ambiguity Resolution (PPP-WAR) model with regional corrections can reach the meter level and the PLs estimated by PPP Ambiguity Resolution (PPP-AR) and PPP-RTK models are usually the sub-meter level. Given a horizontal Alert Limit (AL) of 1.5 m, the global coverage of availability above 99.9% for PPP-WAR, PPP-AR, and PPP-RTK can reach 92.6%, 99.4%, and 99.7% respectively. The results using real kinematic data also show that tight PLs can be achieved when the observation conditions are good.

Keywords Integrity monitoring, Precise point positioning, Multi-GNSS, Ambiguity resolution, Single-epoch positioning

Introduction

With the rapid development of intelligent transport systems including autonomous driving, the requirements for Global Navigation Satellite Systems (GNSS) related integrity monitoring are significantly increasing. Integrity monitoring provides important information including Protection Levels (PLs) which is critical to determine the availability of the GNSS positioning results. When PLs exceed the predefined Alert Limits (ALs), the GNSS positioning results will be considered unreliable, so it is essential to be used in providing safety-related services. Traditional Receiver Autonomous Integrity Monitoring (RAIM) and Advanced Receiver Autonomous Integrity Monitoring (ARAIM) is designed for aeronautical users and are relatively mature (GEAS, 2010; Working Group C, 2016). However, they are designed for Least Squares (LS) and use (smoothed) pseudorange-based GNSS positioning named as Single Point Positioning (SPP) which has usually low accuracy and large PLs (Blanch et al., 2015). It is obvious that they cannot meet the demands of high-accuracy applications (Reid et al., 2019). In recent years, Precise Point Positioning (PPP) services including the precise clock, ephemeris, or even ambiguity resolution enabled biases and regional atmospheric

*Correspondence:
Wenhao Zhang
wenhao.zhang1@unsw.edu.au
University of New South Wales (UNSW), Sydney, Australia

Springer Open

© The Author(s) 2023. **Open Access** This article is licensed under a Creative Commons Attribution 4.0 International License, which permits use, sharing, adaptation, distribution and reproduction in any medium or format, as long as you give appropriate credit to the original author(s) and the source, provide a link to the Creative Commons licence, and indicate if changes were made. The images or other third party material in this article are included in the article's Creative Commons licence, unless indicated otherwise in a credit line to the material. If material is not included in the article's Creative Commons licence and your intended use is not permitted by statutory regulation or exceeds the permitted use, you will need to obtain permission directly from the copyright holder. To view a copy of this licence, visit http://creativecommons.org/licenses/by/4.0/.

corrections are developing significantly. Based on these products, PPP uses not only pseudoranges but also carrier phases for positioning which can generate high precision for localization attributed to the small noise of carrier phase. Nevertheless, the integrity monitoring scheme for PPP is still not mature enough and under investigation. The ARAIM method can be considered as an extension to RAIM method which includes the probability of faults in the assumptions. In ARAIM theory, fault detection, exclusion, and PL estimation can be computed based on different statistics approaches, e.g., Multiple Hypothesis Solution Separation (MHSS), chi-square test, and data snooping. Since it has been shown that MHSS can generate a tighter bound for PLs (Gunning et al., 2018), in this study, we mainly focus on the MHSS-based ARAIM method.

There are many differences between SPP and PPP that prevent the baseline MHSS ARAIM method directly used in PPP. Since the carrier phases contain integer ambiguities, PPP uses the observations at many epochs to estimate the position. This will increase the faults that need to be monitored because the faults in previous epochs may also result in integrity risks at the current epoch (Blanch et al., 2020). In the current research, some authors assumed that all the faults at previous epochs were perfectly removed (El-Mowafy & Kubo, 2020; Wang et al., 2020); however, it is still an inevitable risk in real applications. Gunning et al. (2018) run multiple parallel Kalman Filters (KFs) for different subsets to monitor faults. This method is theoretically equivalent to implementing the conventional MHSS ARAIM method using full LS where faults are grouped by each satellite in a period. Considering that any faults in the same satellite during the period will be considered as a fault event (Gunning et al., 2018), this will lead to a high probability of fault and finally result in a large number of subsets and severe computational burden, unless the fault rate is very low. Meanwhile, time-correlated errors may exist in the multiple epochs of measurements, which may not be considered in the nominal error model (Zhang et al., 2023).

Such time-correlated errors may be considered to reduce the probabilities of detected faults caused by them; thus, extra parameters following a first-order Gauss-Markov process are added to model the time-correlated errors (Racelis & Joerger, 2020). This method can solve the existing issues of time-correlated errors in dual-frequency float PPP to some extent; nevertheless, it is more complex in multi-frequency or undifferenced models or PPP ambiguity-fixed scenarios. This is because the time-correlated errors may be both frequency-dependent and frequency-independent and temporal correlations may not follow the first-order Gauss-Markov process.

Considering that these problems are mainly caused by using measurements from previous epochs based on the banks of KFs (Zhang et al., 2023), it is, therefore, reasonable thinking to find an applicable strategy that avoids using the measurements of the previous epochs for PPP integrity monitoring. Inspired by the research of instantaneous PPP (Geng & Guo, 2020; Geng et al., 2019; Laurichesse & Banville, 2018), only fixed ambiguities and measurements at this epoch can be used to estimate the positions with strong model strength. An integrity monitoring scheme can be designed under the single-epoch PPP Real-Time Kinematic (RTK) framework to reduce the number of simultaneous faults and avoid involving the temporal correlations between measurements of different epochs because only measurements of this epoch are used in the estimator. In this contribution, we study the ARAIM method for the PPP model under the single-epoch PPP-RTK framework which only uses the observations at a single epoch. For real single epoch models, the ARAIM method can be easily implemented, and for the models not achievable in real single epoch solutions, a scheme is also proposed to implement under this framework. A filter can be processed as the conventional PPP-Ambiguity Resolution (PPP-AR) or PPP-RTK model, and the ambiguity resolution results of this parallel filter can be processed with the observations at the current epoch as pseudo-single-epoch PPP-RTK to estimate the PLs. In addition, fault models are analyzed and discussed. Besides, global performance with different scenarios is also investigated based on the simulation results computed by the precise satellite ephemeris to present the potential of this scheme.

Models and methods

Baseline MHSS ARAIM method

In the MHSS ARAIM framework for the LS, the first step is to determine the maximum number of the simultaneously monitored event of faults based on the given threshold.

$$\begin{aligned} \min_{N_{\max-\text{event}}} &= [P(N_{\text{number of events}} > N_{\max-\text{event}})] \\ &= P_{\text{unmonitored}} < P_{\text{threhold}} \end{aligned} \tag{1}$$

where $P(*)$ is the notation of probability; P_{threhold} is the predefined threshold for unmonitored probabilities; $N_{\text{max - event}}$ is the maximum number of simultaneous faults that need to be monitored.

The details for computing the unmonitored probabilities can refer to Blanch et al. (2012). When the number of

simultaneous monitored events of faults is estimated, the subsets of fault events can be generated with the probability of each subset. Some subsets that cannot be used to compute the position should be also filtered out in this step (Working Group C, 2016). Besides, the optimization method of monitored subsets can also be implemented to improve the performance at this stage (Meng et al., 2019). This method will remove some of the subsets which have small probabilities and make the probabilities of unmonitored faults close but not exceed the threshold of the probabilities of unmonitored faults.

Then the results of subset solutions and all-in-view solutions can be solved by the LS which yields:

$$\hat{x}^{(k)} = \left(\boldsymbol{A}^{\mathrm{T}}\boldsymbol{W}^{(k)}\boldsymbol{A}\right)^{-1}\boldsymbol{A}^{\mathrm{T}}\boldsymbol{W}\boldsymbol{l} \tag{2}$$

$$\boldsymbol{W} = \boldsymbol{R}^{-1} \tag{3}$$

where $(*)^{(k)}$ is the notation of the k th subsets and 0 indicates the all-in-view solution; R is the variance–covariance matrix of measurements; $\boldsymbol{A}$ is the design matrix based on satellite geometry; $\boldsymbol{l}$ is the observation minus computation (O-C) vector and $\hat{x}$ is the estimated results.

The variance–covariance matrix for the estimated parameters is written as:

$$\boldsymbol{R}_{\hat{x}}^{(k)} = \left(\boldsymbol{A}^{\mathrm{T}}\boldsymbol{W}^{(k)}\boldsymbol{A}\right)^{-1} \tag{4}$$

Based on the results for the subsets and all-in-view solutions, the MHSS approach can be implemented for fault detection and exclusion with the estimated thresholds as (Blanch et al., 2012):

$$T_{k,q} = K_{\mathrm{FA},q}{}^{(k)}\sigma_{\mathrm{SS},q} \tag{5}$$

$${}^{(k)}\sigma^2_{\mathrm{SS},q} = {}^{(k)}\sigma^2_q - {}^{(0)}\sigma^2_q \tag{6}$$

$$K_{\mathrm{FA},1} = K_{\mathrm{FA},2} = \boldsymbol{Q}^{-1}\left(\frac{P_{\mathrm{FA\_Horizontal}}}{4N}\right) \tag{7}$$

$$K_{\mathrm{FA},3} = \boldsymbol{Q}^{-1}\left(\frac{P_{\mathrm{FA\_vertical}}}{2N}\right) \tag{8}$$

where $T_{k,q}$ is the threshold of the Solution Separation Test (SST); k represents the k th subsets and 0 represents the all-in-view solution; $q = 1, 2, 3$ indicate the estimated coordinates in the east, north, and vertical directions, respectively, in the local coordinate system; σ^2 is the variance of the estimated unknown which can be extracted from the variance–covariance matrix of estimated results; $\boldsymbol{Q}^{-1}(p)$ is the quantile of the standard normal distribution for $(1-p)$; $P_{\mathrm{FA\_vertical}}$ and $P_{\mathrm{FA\_Horizontal}}$ are the given false alarm probabilities (expected continuity risks) in the vertical and horizontal directions, respectively; N is the number of subsets.

The absolute value of the difference between subset solutions $x_q^{(k)}$ and all-in-view solutions $x_q^{(0)}$ will be used for fault detection, it is considered containing faults when

$$\left|x_q^{(k)} - x_q^{(0)}\right| > T_{k,q} \tag{9}$$

The PL is defined as:

$$\sum P\left(\delta_{\text{position error}} > \delta_{\text{PL\&test passed}}\right)P\left(\delta_{\text{fault occurance}}\right) < D_{\mathrm{PHMI}} \tag{10}$$

which can be further derived as:

$$\sum_{i=0}^{N} P(\left|x - \hat{x}\right| > \delta_{\mathrm{PL}\&y\in\Omega|H_i})P(H_i) < D_{\mathrm{PHMI}} \tag{11}$$

where x and $\hat{x}$ are the state and all-in-view estimated state; H_i is the hypothesis i; and Ω is the measurement region based on the test statistics. Except for the Gaussian noise, nominal biases are also considered to exist in the fault-tolerant model (Blanch et al., 2012). It can be easy to understand that the largest impact caused by these nominal biases will happen when they have the same sign for projecting to the estimated positions, which yields:

$$b^{(k)} = \left|\left(\boldsymbol{A}^{\mathrm{T}}\boldsymbol{W}^{(k)}\boldsymbol{A}\right)^{-1}\boldsymbol{A}^{\mathrm{T}}\boldsymbol{W}^{(k)}\right|b_{\mathrm{nominal}} \tag{12}$$

where b_{nominal} is the largest scale of nominal bias vector and $b^{(k)}$ is the vectors of the largest impact caused by the nominal biases. An upper bound of PL can be computed using the half interval search for the q component as (Blanch et al., 2012):

$$\left\{2Q\left(\frac{\alpha_{\mathrm{PL}} - b^{(0)}}{{}^{(0)}\delta}\right) + \sum_{i=0}^{N} Q\left(\frac{\alpha_{\mathrm{PL}} - T_i - b^{(0)}}{{}^{(i)}\delta}\right)P(H_i) = D_{\mathrm{PHMI}}\right\}_q \tag{13}$$

where Q is the cumulative distribution function of the standard normal distribution.

GNSS models

For multi-frequency multi-constellation GNSS processing, the linearized pseudorange and carrier phase observations can be expressed as:

$$\begin{aligned}\mathrm{E}\left(P_{r,j}^s\right) =& {}^{(0)}\rho_r^s + \boldsymbol{G}_r^s\boldsymbol{u}_r + c\left(\mathrm{d}t_{r,\mathrm{sys}} - \mathrm{d}t^s\right) \\ &+ b_{r,\mathrm{sys},j} - b_j^s + M_r^s Z_r + \mu_j I_{r,1}^s\end{aligned} \tag{14}$$

$$\begin{aligned}\mathrm{E}\left(L_{r,j}^{s}\right) = {}^{(0)}\rho_{r}^{s} + \boldsymbol{G}_{r}^{s}\boldsymbol{u}_{r} + c\left(\mathrm{d}t_{r,\mathrm{sys}} - \mathrm{d}t^{s}\right) \\ + \lambda_{j}\left(N_{r,j}^{s} + B_{r,\mathrm{sys},j} - B_{j}^{s}\right) \\ + M_{r}^{s}Z_{r} - \mu_{j}I_{r,1}^{s}\end{aligned} \tag{15}$$

where $P_{r,j}^{s}$ and $L_{r,j}^{s}$ represent the measurements of pseudorange and carrier phase observations on frequency j for the respective satellite s and receiver r pair respectively; $\mathrm{E}(*)$ denotes the expectation operator, $\boldsymbol{G}_{r}^{s}$ is the unit vectors matrix from the receiver to the satellite and $\boldsymbol{u}_{r}$ is the position increments from estimated positions to the linearized point; sys identify the constellation; ${}^{(0)}\rho_{r}^{s}$ is the distance between respective satellite and receiver pair; ${}^{(0)}\rho_{r}^{s}$ and $\mathrm{d}t$ are the speed of light and time offsets respectively; λ_{j} is the wavelength on frequency j and $N_{r,j}^{s}$ is the integer ambiguity; $b_{r,\mathrm{sys},j}$ and b_{j}^{s} denote the hardware on receiver end and satellite end, respectively; $B_{r,\mathrm{sys},j}$ and B_{j}^{s} denote the phase delay on receiver end and satellite end, respectively; Z_{r} is the zenith tropospheric delay and M_{r}^{s} is the mapping function from zenith to slant direction; μ_{j} is the frequency-dependent scaling coefficients from frequency 1 to j which equals to $\frac{f_{1}^{2}}{f_{2}^{2}}$ and I_{1} represent the ionospheric delay at the first frequency. It is assumed that other biases are priorly corrected by models.

It is clear that the receiver clock, satellite biases, receiver biases, integer ambiguities, satellite phase biases, and receiver phase biases are linearly dependent; thus, they cannot be solved simultaneously. Therefore, they are usually lumped as new parameters with the full rank which yields:

$$\begin{aligned}\mathrm{E}\left(\hat{P}_{r,j}^{s}\right) = &\boldsymbol{G}_{r}^{s}\boldsymbol{u}_{r} + c\mathrm{d}\bar{t}_{r,\mathrm{sys}} - c\mathrm{d}\bar{t}_{j}^{s} + \bar{b}_{r,\mathrm{sys},j} \\ &- \bar{b}_{j}^{s} + M_{r}^{s}Z_{r} + \mu_{j}\tilde{I}_{r,1}^{s}\end{aligned} \tag{16}$$

$$\mathrm{E}\left(\hat{L}_{r,j}^{s}\right) = \boldsymbol{G}_{r}^{s}\boldsymbol{u}_{r} + c\mathrm{d}\bar{t}_{r,\mathrm{sys}} - c\mathrm{d}\bar{t}_{j}^{s} + \lambda_{j}\tilde{N}_{r,j}^{s} + M_{r}^{s}Z_{r} - \mu_{j}\tilde{I}_{r,1}^{s} \tag{17}$$

$$\begin{cases}\hat{P}_{r,j}^{s} = P_{r,j}^{s} - {}^{(0)}\rho_{r}^{s} \\ \hat{L}_{r,j}^{s} = L_{r,j}^{s} - {}^{(0)}\rho_{r}^{s} \\ c\mathrm{d}\bar{t}_{r,\mathrm{sys}} = c\mathrm{d}t_{r,\mathrm{sys}} + b_{r,\mathrm{sys,IF}} \\ c\mathrm{d}\bar{t}_{j}^{s} = c\mathrm{d}t_{j}^{s} + b_{\mathrm{IF}}^{s} \\ \bar{b}_{r,\mathrm{sys},j} = \begin{cases} 0 & (j \le 2) \\ b_{r,\mathrm{sys},j} - \mu_{j}\frac{f_{2}^{2}}{f_{1}^{2}-f_{2}^{2}}b_{r,\mathrm{sys,GF}} - b_{r,\mathrm{sys,IF}} & (j > j) \end{cases} \\ \bar{b}_{j}^{s} = \begin{cases} 0\,(j \le 2) \\ b_{\mathrm{sys},j}^{s} - \mu_{j}\frac{f_{2}^{2}}{f_{1}^{2}-f_{2}^{2}}b_{\mathrm{GF}}^{s} - b_{\mathrm{IF}}^{s}\,(j > 2) \end{cases} \\ \lambda_{j}\tilde{N}_{r,j}^{s} = \lambda_{j}N_{r,j}^{s} + \lambda_{j}B_{r,\mathrm{sys,IF}} + b_{r,\mathrm{sys,IF}} + \mu_{j}\frac{f_{2}^{2}}{f_{1}^{2}-f_{2}^{2}}b_{r,\mathrm{sys,GF}} \\ -\lambda_{j}B_{j}^{s} - b_{\mathrm{IF}}^{s} - \mu_{j}\frac{f_{2}^{2}}{f_{1}^{2}-f_{2}^{2}}b_{\mathrm{GF}}^{s} \\ \tilde{I}_{r,1}^{s} = I_{r,1}^{s} + \frac{f_{2}^{2}}{f_{1}^{2}-f_{2}^{2}}b_{r,\mathrm{sys,GF}} - \frac{f_{2}^{2}}{f_{1}^{2}-f_{2}^{2}}b_{\mathrm{GF}}^{s}\end{cases} \tag{18}$$

where $c\mathrm{d}\bar{t}_{r,\mathrm{sys}}$ and $c\mathrm{d}\bar{t}_{j}^{s}$ are receiver and satellite clock offset absorbed part of biases respectively; $\bar{b}_{r,\mathrm{sys},j}$ and $\bar{b}_{j}^{s}$ are Inter-Frequency (IF) Clock Biases (CBs) for receiver and satellite respectively; $\tilde{I}_{r,1}^{s}$ are the new ionospheric delays and $\tilde{N}_{r,j}^{s}$ is the new ambiguities absorbed the rest of the biases.

From Eq. (18), we can therefore notice that the newly grouped ambiguity parameters lost their integer nature because they are contaminated by the satellite and receiver biases. As a result, these biases should be solved before ambiguity resolutions. For satellite-respect biases, they can be estimated by the Uncalibrated Phase Delay (UPD) method (Ge et al., 2008) or Integer Recovery Clock (IRC) method/ Decoupled Satellite Clock (DSC) method (Collins, 2008; Collins et al., 2008; Laurichesse et al., 2009; Loyer et al., 2012). It has been proven that UPD and IRC methods are theoretically equivalent. When the hardware bias is available, these UPDs or IRCs can be recovered into undifferenced fractional parts to correct the grouped ambiguity parameters for eliminating the impact of satellite biases.

$$\mathrm{E}\left(\hat{P}_{r,j}^{s}\right) = \boldsymbol{G}_{r}^{s}\boldsymbol{u}_{r} + c\mathrm{d}\bar{t}_{r,\mathrm{sys}} + \bar{b}_{r,\mathrm{sys},j} + M_{r}^{s}Z_{r} + \mu_{j}\bar{I}_{r,1}^{s} \tag{19}$$

$$\mathrm{E}\left(\hat{L}_{r,j}^{s}\right) = \boldsymbol{G}_{r}^{s}\boldsymbol{u}_{r} + c\mathrm{d}\bar{t}_{r,\mathrm{sys}} + \lambda_{j}\bar{N}_{r,j}^{s} + M_{r}^{s}Z_{r} - \mu_{j}\bar{I}_{r,1}^{s} \tag{20}$$

$$\begin{cases} c\mathrm{d}\bar{t}_{r,\mathrm{sys}} = c\mathrm{d}t_{r,\mathrm{sys}} + b_{r,\mathrm{sys,IF}} \\ \bar{b}_{r,\mathrm{sys},j} = \begin{cases} 0 & (j \le 2) \\ b_{r,\mathrm{sys},j} - \mu_{j}\frac{f_{2}^{2}}{f_{1}^{2}-f_{2}^{2}}b_{r,\mathrm{sys,GF}} - b_{r,\mathrm{sys,IF}} & j > 2 \end{cases} \\ \lambda_{j}\bar{N}_{r,j}^{s} = \lambda_{j}N_{r,j}^{s} + \lambda_{j}B_{r,\mathrm{sys},j} + b_{r,\mathrm{sys,IF}} + \mu_{j}\frac{f_{2}^{2}}{f_{1}^{2}-f_{2}^{2}}b_{r,\mathrm{sys,GF}} \\ \bar{N}_{r,1}^{s} = I_{r,1}^{s} + \frac{f_{2}^{2}}{f_{1}^{2}-f_{2}^{2}}b_{r,\mathrm{sys,GF}} \end{cases} \tag{21}$$

Uncombined PPP-RTK models can also refer to other studies using a regional network (e.g., Zhang et al., 2011, 2019). For the receiver-respect biases, it can be noticed that they are identical for the signals in the same constellation with the same frequency. Therefore, these fractional parts caused by receiver-respect biases could be eliminated by single-differencing or selecting datum methods. These two methods are also theoretically equivalent, and in this study, the single-differencing method is used which yields:

$$\bar{N}_{r,j}^{p} - \bar{N}_{r,j}^{q} = N_{r,j}^{p} - N_{r,j}^{q} = N_{r,j}^{pq} \tag{22}$$

where $(*)^{q}$ is the notation of the reference satellite and $(*)^{p}$ is the notation of other normal satellites. $(*)^{pq}$ is the notation of between-satellite differencing.

Meanwhile, directly fixing all ambiguities at the same time will be difficult, because the wavelength is relatively small compared to the pseudorange noise. Therefore, ambiguities are usually fixed sequentially in Extra-Wide-Lane (EWL), Wide-Lane (WL), and Narrow-Lane (NL) order, which yields:

$$\begin{cases} N_{r,\mathrm{WL}}^{pq} = N_{r,2}^{pq} - N_{r,1}^{pq} \\ N_{r,\mathrm{EWL},j}^{pq} = N_{r,j}^{pq} - N_{r,2}^{pq} \end{cases} \tag{23}$$

With NL:

$$N_{r,\mathrm{NL}}^{pq} = N_{r,1}^{pq} \tag{24}$$

where $N_{r,\mathrm{NL}}^{pq}$, $N_{r,\mathrm{WL}}^{pq}$, $N_{r,\mathrm{EWL},j}^{pq}$ are the between-satellite differenced NL, WL, EWL ambiguities, respectively.

Thus, the single-differenced original ambiguities can be written as:

$$\begin{cases} N_{r,2}^{pq} = N_{r,1}^{pq} + N_{r,\mathrm{WL}}^{pq} \\ N_{r,j}^{pq} = N_{r,1}^{pq} + N_{r,\mathrm{WL}}^{pq} + N_{r,\mathrm{EWL},j}^{pq} \end{cases} \tag{25}$$

Except for the raw GNSS observations, regional atmospheric corrections and tropospheric corrections can be also used to improve the performance of PPP-RTK.

$$Z_r = Z_{r,\mathrm{interpolate}} \tag{26}$$

$$\bar{I}_{r,1}^{pq} = I_{r,\mathrm{interpolate}}^{pq} \tag{27}$$

where $(*)_{r,\mathrm{interpolate}}$ is the regional correction interpolated at the user's location.

Different processing methods based on GNSS observations and corrections

Since the ARAIM scheme is applicable for a least squares estimator for integrity monitoring where measurements may have faults. Therefore, it will be also applicable for the single-epoch PPP-RTK positioning using the least squares, with pseudoranges, carrier phases, and the ionospheric and tropospheric corrections as pseudo-measurements. In the framework of single-epoch processing, the difference between different positioning models is only the use of different types of measurements. Measurements including both observations and pseudo-observations in different models including SPP, PPP Wide-lane Ambiguity Resolution (PPP-WAR), PPP-WAR with atmospheric corrections which can also be considered as PPP-RTK only fixing WL ambiguities, PPP-AR, and PPP-RTK are listed in Table 1.

Table 1 Measurements used in different positioning models

Methods	Measurements
SPP	(19)
PPP-WAR	(19) (20) (21)
PPP-WAR with atmospheric corrections	(19) (20) (23) (26) (27)
PPP-AR	(19) (20) (23) (24)
PPP-RTK	(19) (20) (23) (24) (26) (27)

These models can be used for different scenarios. For example, PPP-WAR has been proven to be achievable in real instantaneous (single-epoch) positioning (Geng & Guo, 2020; Geng et al., 2019). However, PPP-AR is difficult to achieve if only single-epoch observations are available. Even Laurichesse and Banville (2018) have some experimental results in single-epoch PPP-AR based on a small-scale network for two systems, no other research has been seen to achieve conventional PPP-AR in a single epoch. While some results showed that it can in achieved after a few epochs (Tao et al., 2022). It is encouraging that the PPP-AR might be achievable in the future with the increase of model strength in both geometry and frequencies.

In this study, this framework only aims at monitoring the integrity of the positioning results. Therefore, there is no necessity to achieve real single-epoch ambiguity fixing in the application. A filter is used to process as the conventional PPP-AR or PPP-RTK model and ambiguities fixing information can be obtained by this conventional PPP-AR or PPP-RTK filter. This ambiguity-fixing information can be considered as additional corrections and be used in the parallel single-epoch PPP-AR or PPP-RTK estimator which is similar to the fix and hold strategy in ambiguity fixing. The flowchart shown in Fig. 1 presents an applicable scheme for the results that cannot be processed in a real single-epoch solution. When ambiguities are not fixed, this model can be downgraded to single-epoch PPP-WAR if only wide-lane ambiguities are fixed or even SPP.

Fault models

In the traditional MHSS ARAIM method for SPP, only real GNSS observations are involved in fault events. When it comes to PPP-WAR or even PPP-RTK, more faults may exist in the newly involved measurements including pseudo-measurements for fixed ambiguities and atmospheric corrections. Therefore, it is necessary to define a more general fault event model in this scenario.

Meanwhile, from Eq. (22–27), it can be noticed the reference satellite and other satellites are distinct in these measurements which is different from SPP. The effects of single-differencing mainly include implementing ionospheric corrections and ambiguity resolution. To solve this issue, we assume that the fault events for these

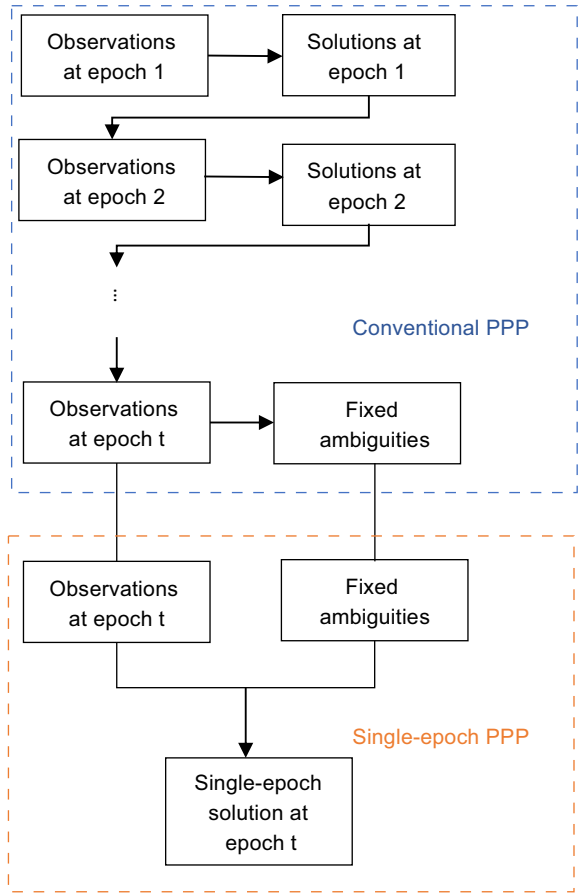

Fig. 1 Scheme for conventional PPP-RTK to single-epoch PPP-RTK framework

single-differenced measurements still exist in the undifferenced measurements. This means that the subsets for excluding the reference satellite will generate single-differenced measurements with a new reference satellite because single-differencing measurements can be written as all undifferenced measurements with an extra random term, which yields:

$$(*)^{p}_{r,j} - (*)^{q}_{r,j} = (*)^{pq}_{r,j} \Leftrightarrow (*)^{s}_{r,j} - \xi = (*)^{pq}_{r,j} \tag{28}$$

where ξ is the extra random term. It is obvious that one more measurement and one more unknown are added in this transformation.

Considering that all measurements may contain faults, in this study, fault events including but not limited to the satellite-related fault and constellation fault in the traditional ARAIM are illustrated based on the observation and pseudo-observation types. Therefore, the fault models under this framework can be summarized in Table 2.

In this study, the risks of incorrect ambiguity fixing are considered as ignorable. While this assumption is widely used in existing studies (Jokinen et al., 2013a; Jokinen et al., 2013b; Feng et al., 2014; Wang et al., 2020; Wang et al. 2022; Gao et al., 2021), the effects of wrong ambiguity fixing on the protection level computations are analyzed in Sect."Effects of fault probabilities on protection level computations".

Numerical experiment

Experimental settings

To evaluate the performance of the proposed methods for these different models with ARAIM methods, we reveal the most ideal performance results globally. In this simulation, all ambiguities are considered fixed, all satellites are observed, and corrections are always available. User positions are simulated with a variation of 10 by 10 degrees based on the precise orbit products on the Day of the Year (DOY) 01 in 2022 and the time step is set to 300 s.

Before the implementation, stochastic models, fault probabilities, PHMI, and false alarm rates should be defined priorly. Based on the existing research (Blanch et al., 2015; Racelis & Joerger, 2020; Wang et al., 2022; Working Group C, 2016), these parameters are set as in Table 3. It is worth mentioning that nominal biases and standard deviations of uncombined observations are still under investigation, we use a conservative setting which is usually used for IF combinations for them. IF combination will amplify the noise with the combination (Richert and EI-Sheimy, 2007), and thus, if uncombined observations and IF combinations share the same level of noise, it means the stochastic model for uncombined observations is more conservative. Priority probabilities and stochastic models for PPP-RTK will vary with different augmentation systems, different working environments and even different receivers, so they still need further

Table 2 Fault models for different measurements

Fault events	Descriptions	Name for fault probability	Affected measurements (group methods)
Satellite-related fault	Prior fault probability of satellite per approach	$P_{\text{sat},i}$	(19) (20)
Constellation fault	Prior fault probability of constellation per approach	$P_{\text{const},j}$	(19) (20)
Ionospheric correction fault	Prior fault probability of ionospheric correction per approach	$P_{\text{iono},i}$	(26)
Tropospheric correction fault	Prior fault probability of tropospheric correction per approach	P_{trop}	(27)

Table 3 List of processing parameters

Parameters	Value
$P_{sat,i}$	1×10^{-5}
$P_{const,j}$	1×10^{-8}
$P_{iono,i}$	1×10^{-5}
P_{trop}	1×10^{-6}
$\sigma_{URE,pseudorange}$	1 m
$\sigma_{URE,phase}$	1/100×
$\sigma_{URE,iono}$	0.06 m
$\sigma_{URE,trop}$	0.03 m
$b_{nominal\ (pseudorange\ and\ phase)}$	3/4× σ_{URE}
$P_{threshold}$	6×10^{-8}
D_{PHMI}	1×10^{-7}
$D_{PHMI\ horizontal}$	2×10^{-9}
$D_{PHMI\ verical}$	9.8×10^{-8}
$P_{FA\ verical}$	3.9×10^{-6}
$P_{FA\ horizontal}$	0.9×10^{-7}

research for real implementation. In addition, at the PPP-RTK user end, preprocessing and quality control section can easily remove a large part of potential faults in these sections; thus, the priority probabilities vary with different processing strategies.

In the traditional ARAIM assumption for (smoothed) pseudorange-based positioning, faults of satellites and constellations are considered as independent by using the nominal error model for considering both noise and bias (Working Group C, 2016).

Considering that we aim to investigate the performance of multiple-frequency multiple-GNSS, we simulate triple-frequency observations for Global Positioning System (GPS), Galileo navigation satellite system (Galileo), and BeiDou Navigation Satellite System (BDS). The Geostationary Earth Orbit (GEO) satellites of BDS are removed from the simulation and Block IIR satellites for GPS only have dual-frequency signals. Meanwhile, it has been proven that using different third frequencies can result in a different performance in convergence and instantaneous PPP (Li et al., 2014). This is because of the different wavelengths and different noise amplification caused by the coefficient related to the wavelength. In addition, to make the simulation close to the real situation, a higher cut-off angle is used in the study. The details are shown in Table 4.

Table 4 GNSS simulation configuration

GPS signals	L1/L2/L5
Galileo signals	E1/E5a/E6
BDS signals	B1/B2/B3
Cut off angle	15°

Numerical analysis for ideal performances

First, the SPP and PPP-WAR methods are analyzed because they are recognized to be achievable under real single-epoch conditions without using regional corrections. Figure 2 presents the estimated PLs for SPP and PPP-WAR respectively. Based on the Alert Limit (AL) with Vertical AL (VAL) of 40 m and Horizontal AL (HAL) of 35 m by LPV-200 (DeCleene, 2006), the availabilities are shown in Fig. 3 for SPP and PPP-WAR.

It is noticed that PLs estimated by these two methods reach tens of meters. Even though the PPP-WAR method has significant improvement compared to the SPP method, results are still not very ideal. As mentioned before, this is because the undifferenced stochastic models are defined based on the widely-used IF stochastic model and a relatively high cut-off angle. It is obvious that the performance can be improved if a more optimistic assumption is used.

Since the PPP-WAR is considered to be achievable in a real single-epoch solution even without regional atmospheric correction, it will only be easier to achieve when regional atmospheric corrections are available. PLs for PPP-WAR with regional atmospheric corrections are shown in Fig. 4. It is noticed that they are mainly at meter level which is close to the requirements in intelligent transport systems. In autonomous driving, ALs are usually determined by the longitudinal and lateral direction; however, this requires attitude information which is not available in this experiment. Thus, HAL is set to 1.5 m based on the square root of the sum of squared longitudinal and lateral ALs for freeways (Reid et al., 2019) to assess the availability of this method which is also shown in Fig. 4.

It is noticed that this method can achieve a high availability based on the requirements. In addition, we can notice that in the overall PHMI and the allocated PHMI to the horizontal and the vertical direction in Table 3. Most of the PHMI budgets are allocated to the vertical direction. This is because the integrity setting is designed for aviation propose (Blanch et al., 2015). If we allocate more budgets to the horizontal directions for autonomous driving purposes because the information on horizontal directions for autonomous driving is more important, the HPL can decrease with the current results and finally improve the availability of this requirement.

Different from the models mentioned before, the PPP-AR and PPP-RTK models are rarely achievable in

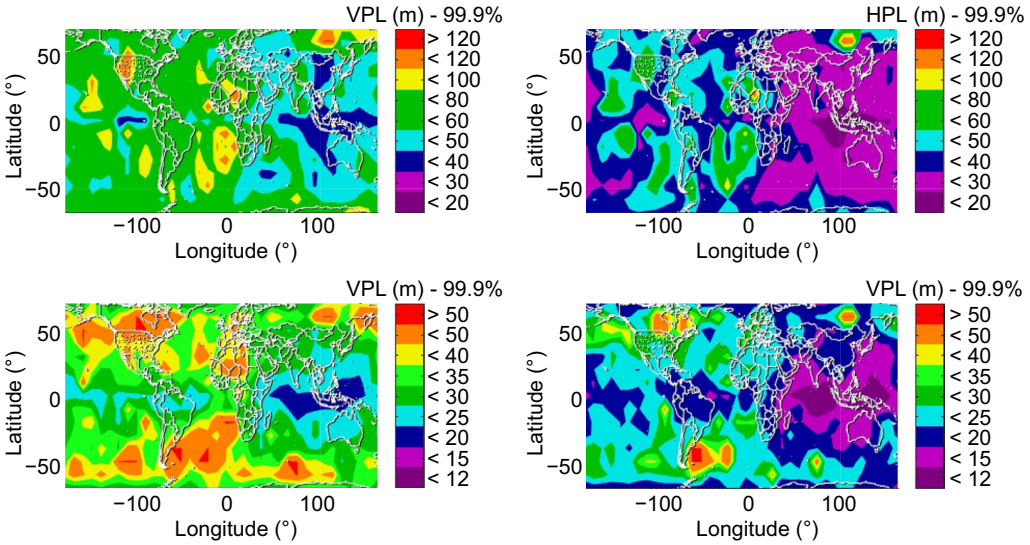

Fig. 2 VPL (top) and HPL (bottom) (right) for SPP model (left) and PPP-WAR model (right) as a function of user location

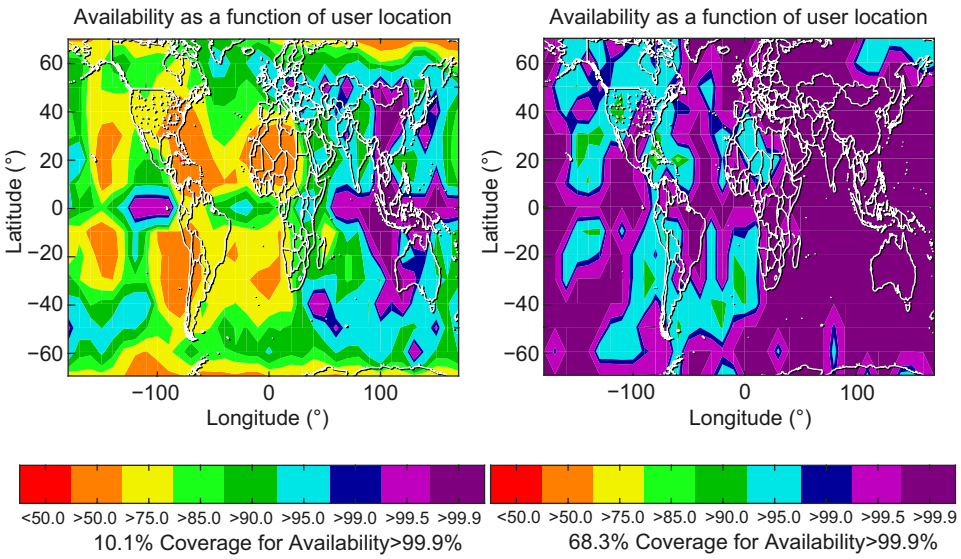

Fig. 3 Availability for SPP model (left) and PPP-WAR model (right) as a function of user location based on VAL = 40 m and HAL = 35 m

real single-epoch performance. These two models have the most accurate solutions because NL ambiguities are fixed into integers. Figure 5 Shows the PLs estimated by the PPP-AR and PPP-RTK models. In most areas, the PLs can even achieve a sub-meter level, and usually meet most of the requirements.

Availability is also assessed based on the aforementioned criteria shown in Fig. 6. These two models can achieve the similar performance and high availabilities with and without regional atmospheric corrections. This does not represent that atmospheric correction is not important because atmospheric corrections can significantly improve the speed of ambiguity-fixing; thus, it is still very critical for positioning.

Kinematic test results

Moreover, in addition to the simulation results, real kinematic datasets were also processed to present the results under the single-epoch framework. These 1 Hz kinematic car-borne datasets were collected in Australia. The details of working environments and trajectories are presented in Fig. 7. Atmospheric corrections

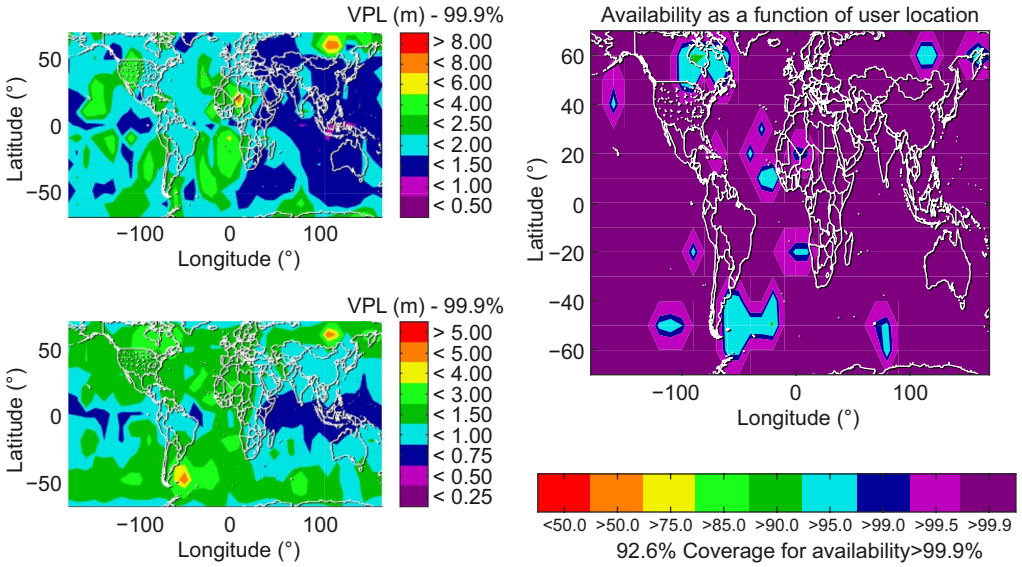

Fig. 4 PL (left) and Availability (right) for PPP-WAR model with regional corrections as a function of user location based on HAL = 1.5 m

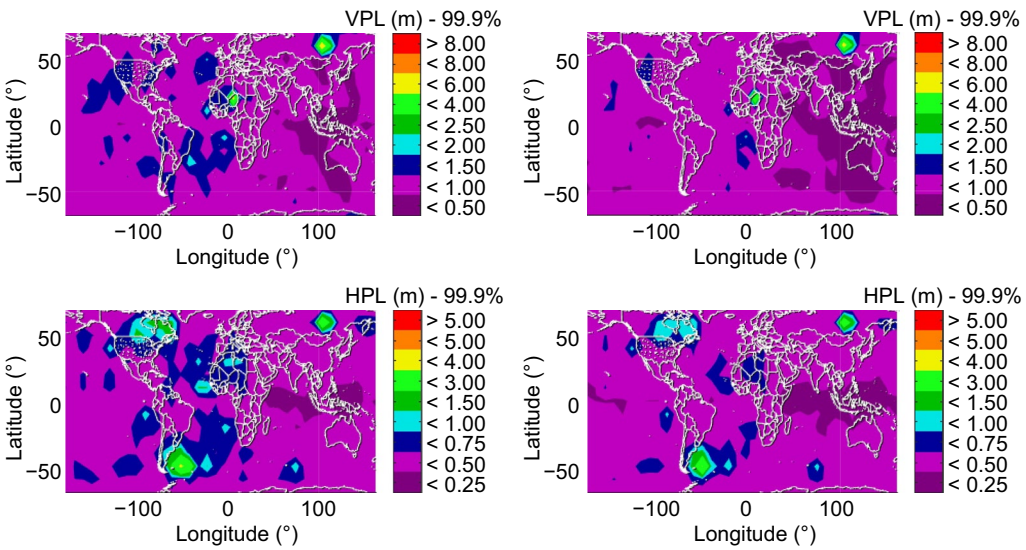

Fig. 5 VPL (top) and HPL (bottom) for PPP-AR (left) and PPP-RTK (right) models as a function of user location

are generated by the nearby reference stations with a lower-order surface model as used by Li et al. (2021).

Since some ambiguities were not fixed in the real processing and some satellites were not tracked by the rover, the geometry and model strength are therefore not as strong as the simulation. The results of Positioning Errors (PEs) of using PPP-WAR model with regional atmospheric corrections, PPP-AR model and PPP-RTK model for these three datasets are illustrated in Figs. 8, 9, 10 respectively. It can be noticed that the PLs estimated by the PPP-WAR model with regional atmospheric corrections can reach a few meters in horizontal direction. The PLs in horizontal directions estimated by the PPP-AR model are in the magnitude of one meter and the PLs in horizontal directions estimated by the PPP-RTK method could reach sub-meter level. At the same time, the positioning errors of PPP-AR and PPP-RTK are at the centimeter level, and PPP-WAR model with atmospheric corrections can reach ten-centimeter level. The magnitude of estimated PL is larger than the positioning errors so that it can protect the positioning error exceeding the estimated PLs. In these cases, all position errors

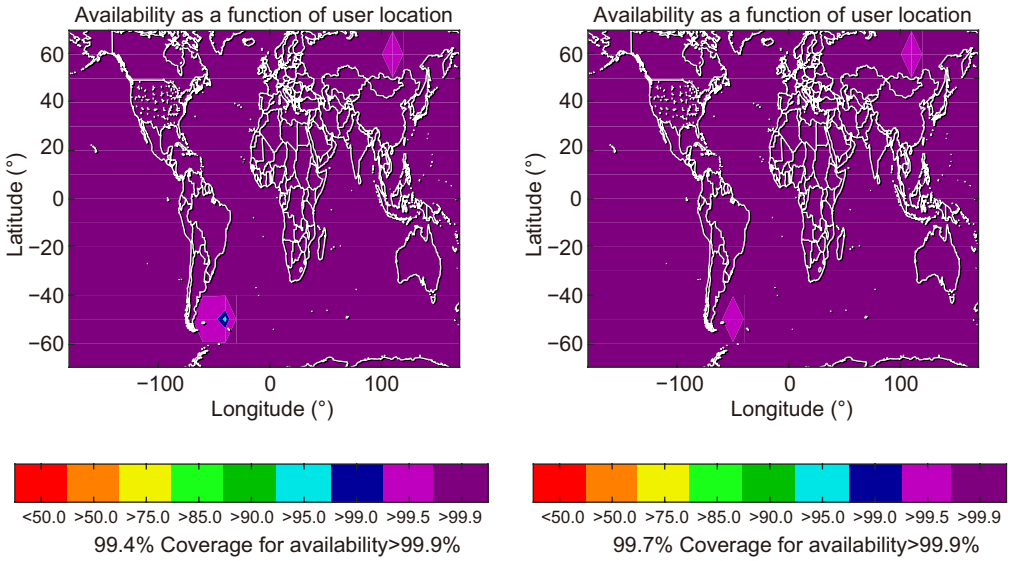

Fig. 6 Availability for PPP-AR (left) and PPP-RTK (right) models as a function of user location based on HAL = 1.5 m

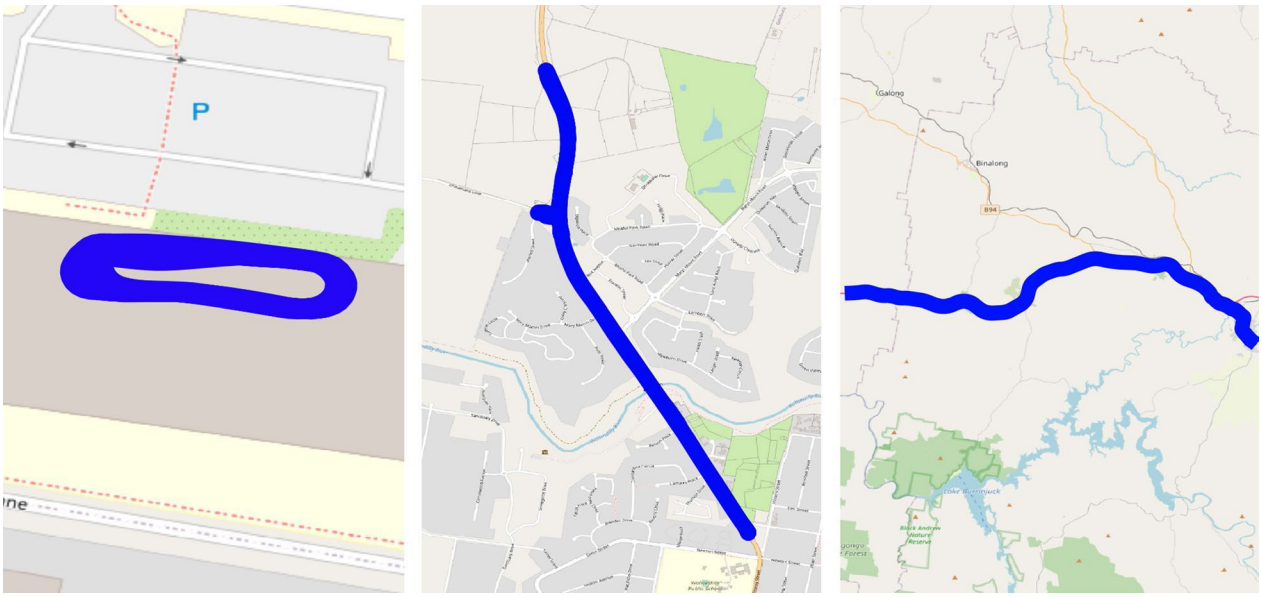

Fig. 7 Trajectories of three kinematic experiment datasets

are properly bounded by the estimated PLs. These case studies demonstrate that this proposed new integrity monitoring method can generate a tight bound in horizontal directions with good observation conditions.

Effects of fault probabilities on protection level computations

Considering the probabilities of different faults are different depending on the different applications, in this section, the effects of different fault probabilities are also investigated. In the previous assumptions, the risks of incorrect ambiguity fixing are ignored therefore, the small probability of incorrect ambiguity fixing is also considered as an unmonitored fault in the case study of the single-epoch PPP-RTK. The probability of incorrect ambiguity fixing with 10^{-8} is tested and the results of the second dataset taken as an example are shown in Fig. 11. It is noticed that the effect is very small (at a few centimeter level).

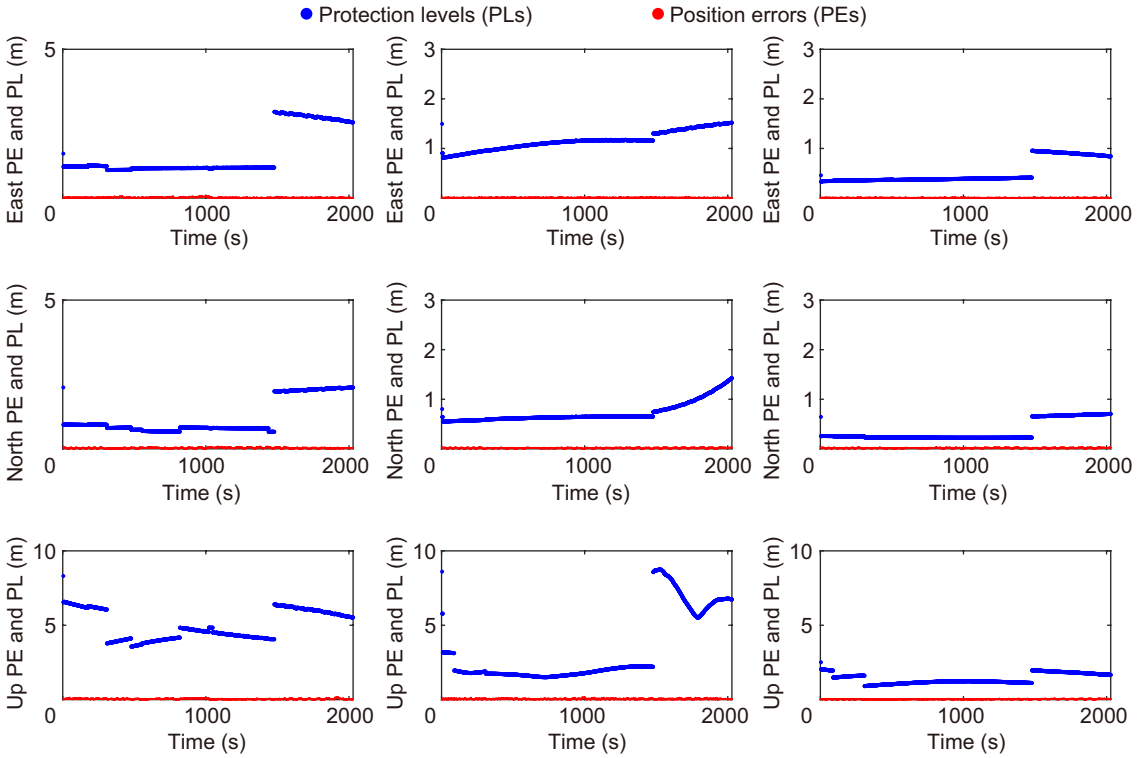

Fig. 8 Performance of the first kinematic dataset for PPP-WAR model with regional atmospheric corrections (left), PPP-AR model (middle), and PPP-RTK model (right)

Moreover, if the probability of incorrect ambiguity fixing increases to 10^{-7}, this method with the same settings is not applicable because the probability of unmonitored faults cannot exceed the PHMI budget. Therefore, in the additional case study below, the PHMI budget is defined as 10^{-6} while the allocation ratios in three directions and other settings are the same as the baseline settings used above. The variations in the protection levels after considering the effect of incorrect ambiguity fixing for three single-epoch PPP positioning scenarios are presented in Fig. 12 and it can be noticed that the effects are still very small.

In addition, the effects of different fault probabilities are investigated with different values based on the baseline settings in Table 3. The estimated PLs of different fault probabilities are presented in Table 5.

It can be noticed that the probabilities of satellite-related faults, constellation faults, and ionospheric correction faults may have significant effects on the estimated PLs in three directions. Differently, the probabilities of tropospheric correction fault will only have significant effects on the estimated vertical PLs. This is because the tropospheric delay parameter is highly correlated with the vertical direction parameter.

While this study focuses on the new integrity monitoring scheme for the single-epoch PPP-RTK positioning scenarios, which can use different probabilities of various faults properly, the probabilities of these faults under various observing conditions will be investigated in the future. Such studies need to collect a large amount of GNSS data sets from real-world application environments.

Summary

The main and most difficult problem of the baseline MHSS ARAIM method used in PPP is mainly caused by multiple epoch observations used in conventional PPP processing. To address this issue, based on the baseline MHSS ARAIM method, we propose a new single epoch PPP-RTK-based scheme for implementation.

This study first discusses the baseline MHSS ARAIM theory and implementation scheme and then analyzes the feasibility of this method based on the single-epoch PPP-RTK framework. At the same time, it presents a practical scheme of the method for models that cannot

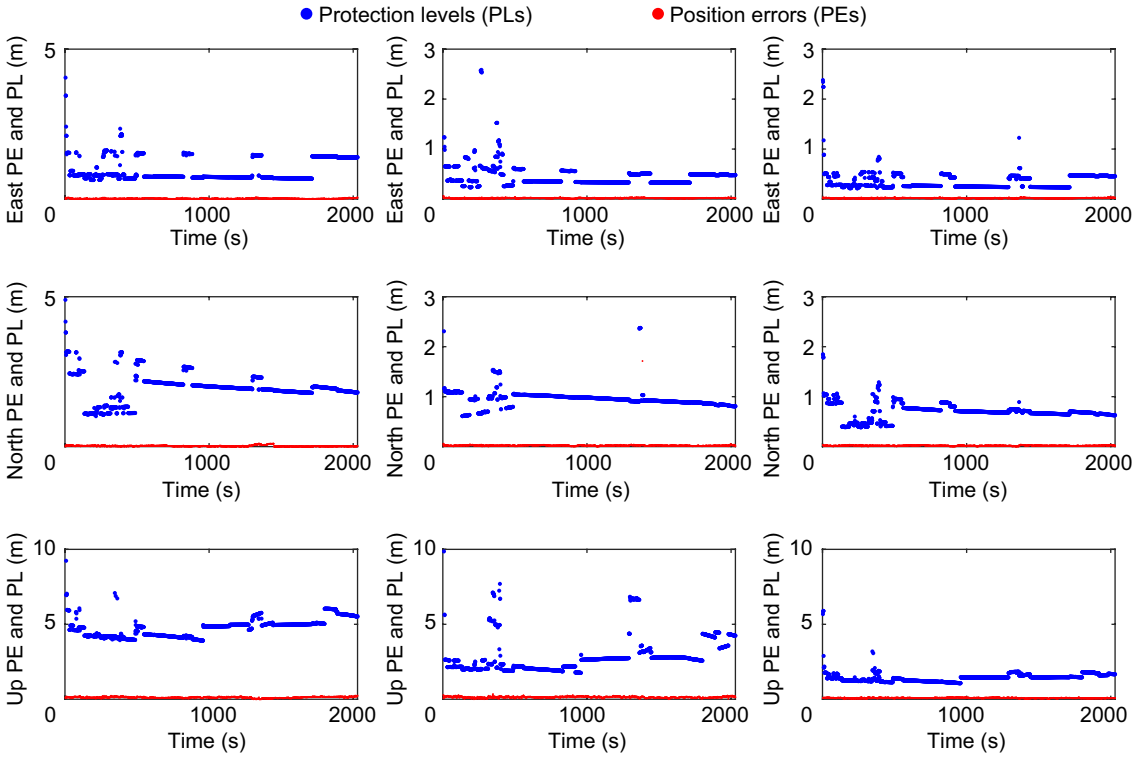

Fig. 9 Performance of the second kinematic dataset for PPP-WAR model with regional atmospheric corrections (left), PPP-AR model (middle), and PPP-RTK model (right)

be achieved in a real single-epoch process. This scheme treats the ambiguity-fixing information obtained by conventional PPP as external corrections that may contain faults and use it in the single-epoch PPP-RTK framework.

For analyzing the potential of ARAIM performance under the single-epoch PPP-RTK framework, ARAIM performances for different single-epoch positioning models are simulated based on real satellite positions. The results show that the PLs obtained by the SPP, and PPP-WAR methods are in the order of ten meters based on this method. The PPP-WAR method with regional atmospheric correction can reach the meter level. For PPP-AR and PPP-RTK models, PLs can usually reach the sub-meter level. This presents the potential of the

Table 5 Median values of estimated PLs (meters) for different fault probabilities

Item	Results of PPP-WAR with regional atmospheric corrections in different directions			Results of Results of PPP-AR in different directions			Results of PPP-RTK in different directions		
	East (E) direction	North (N) direction	Up (U) direction	East (E) direction	North (N) direction	Up (U) direction	East (E) direction	North (N) direction	Up (U) direction
Baseline settings	0.75	1.98	4.92	0.36	0.96	2.64	0.27	0.70	1.47
$P_{sat,i} = 1 \times 10^{-4}$	1.10	2.05	5.09	0.42	1.00	2.91	0.39	0.72	1.51
$P_{sat,i} = 1 \times 10^{-6}$	0.70	0.92	4.92	0.26	0.35	2.43	0.23	0.30	1.46
$P_{const,i} = 1 \times 10^{-7}$	0.82	2.16	4.93	0.38	1.03	4.10	0.29	0.75	1.47
$P_{const,i} = 1 \times 10^{-9}$	0.71	0.95	4.92	0.27	0.37	2.62	0.24	0.33	1.46
$P_{iono,i} = 1 \times 10^{-4}$	1.10	2.05	5.09	0.36	0.96	2.64	0.27	0.72	1.51
$P_{iono,i} = 1 \times 10^{-6}$	0.70	0.92	4.92	0.36	0.96	2.64	0.24	0.32	1.46
$P_{trop,i} = 1 \times 10^{-5}$	0.75	1.98	5.33	0.36	0.96	2.64	0.27	0.70	1.59
$P_{trop,i} = 1 \times 10^{-7}$	0.75	1.98	4.24	0.36	0.96	2.64	0.27	0.70	1.28

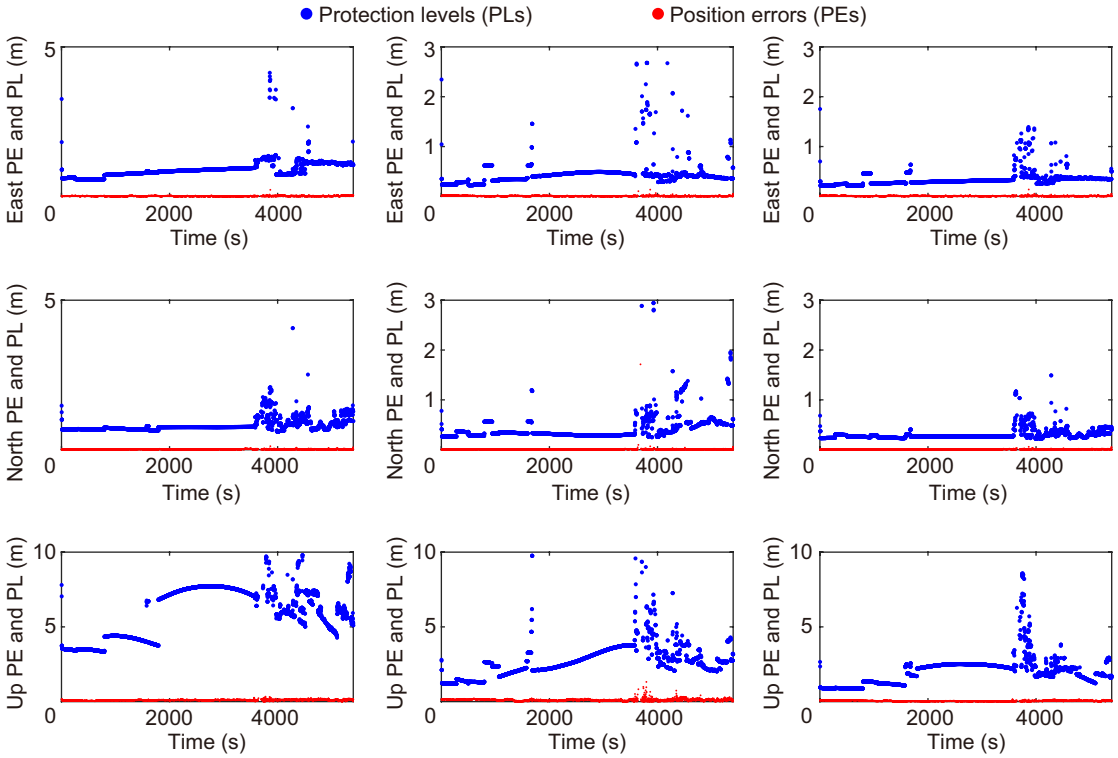

Fig. 10 Performance of the third kinematic dataset for PPP-WAR model with regional atmospheric corrections (left), PPP-AR model (middle), and PPP-RTK model (right)

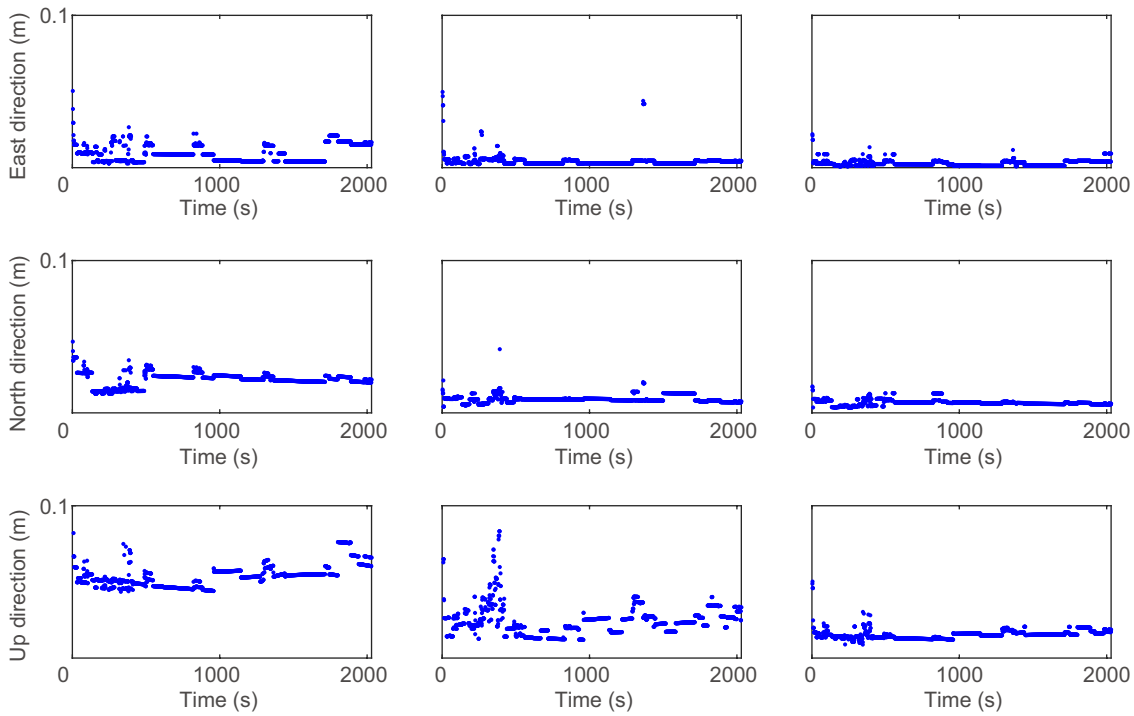

Fig. 11 Variations in the protection levels of the second kinematic dataset for PPP-WAR model with regional atmospheric corrections (left), PPP-AR model (middle), and PPP-RTK model (right) after considering the small probability of incorrect ambiguity fixing (with 10^{-8})

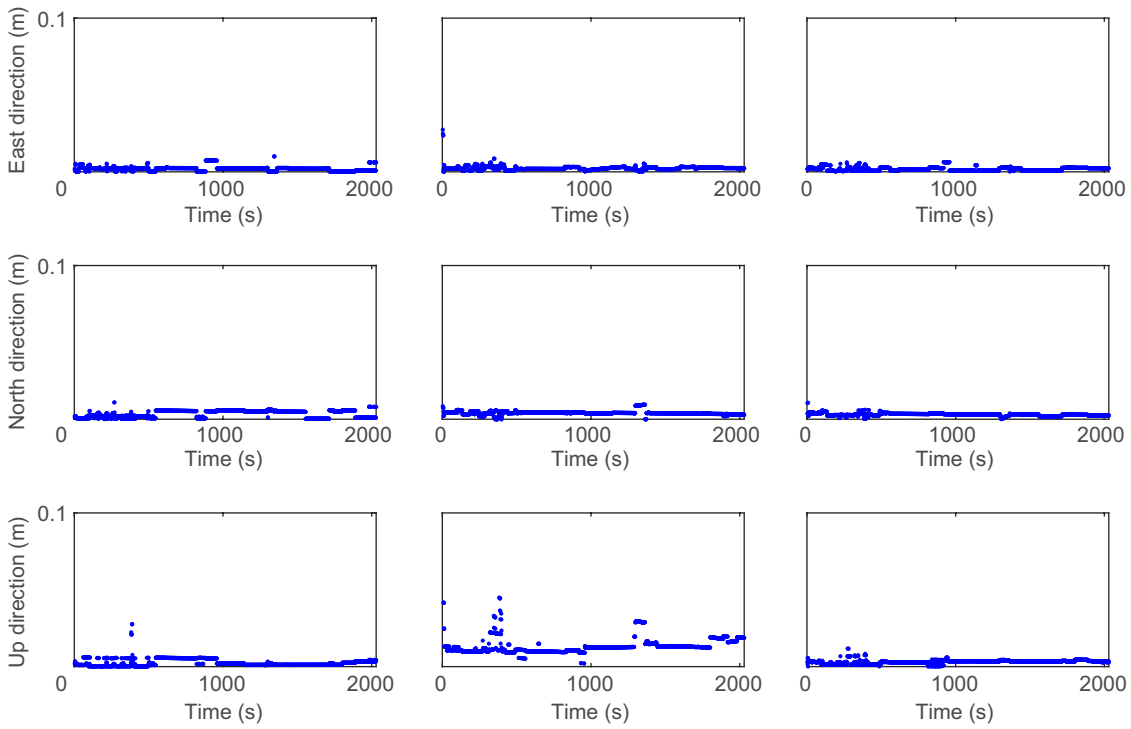

Fig. 12 Variations in the protection levels of the second kinematic dataset for PPP-WAR model with regional atmospheric corrections (left), PPP-AR model (middle), and PPP-RTK model (right) after considering the small probability of incorrect ambiguity fixing (with 1×10^{-7})

method based on the single-epoch PPP-RTK framework in autonomous navigation in the future. Based on the AL of 1.5 m in the horizontal direction, PPP-AR, PPP-RTK or even PPP-WAR with regional corrections have the potential to achieve very high availability for the areas with open sky.

Acknowledgements
The numerical simulation results are estimated based on the modified open-source MATLAB Availability Analysis Simulation Tools (MAAST) developed by the GPS Lab, Stanford University.

Author contributions
WZ designed the research and analyzed the data, WZ and JW contributed to the writing of the paper. Both authors read and approved the final manuscript.

Authors' information
Wenhao Zhang is a Ph.D. graduate from the School of Civil and Environmental Engineering, UNSW, Australia. He obtained his B.Sc. (2016) degree from Sun Yat-sen University, China and M.Sc. (2018) degree from UNSW, Australia. His current research focuses mainly on reliable GNSS precise point positioning and integrity monitoring.
Jinling Wang is an Associate Professor in the School of Civil and Environmental Engineering, UNSW, Australia. His major research interests are in the areas of navigation and geospatial mapping with multi-sensors, such as GNSS, INS, pseudolites, lidar, and cameras. He has published more than 300 papers in journals and conference proceedings, as well as two commercial software packages.

Funding
This research received no specific grant from any funding agency in the public, commercial, or not-for-profit sectors.

Availability of data and materials
The results generated and/or analyzed during the current study are available from the corresponding author on reasonable request.

Declarations

Competing interests
The authors declare that they have no competing interests.

Received: 4 October 2022 Accepted: 3 March 2023
Published online: 03 April 2023

References

Blanch, J., Walter, T., Enge, P., Lee, Y., Pervan, B., Rippl, M., & Spletter, A. (2012). Advanced RAIM user algorithm description: Integrity support message processing, fault detection, exclusion, and protection level calculation. In Proceedings of the 25th International Technical Meeting of the Satellite Division of the Institute of Navigation (ION GNSS 2012) (pp. 2828–2849).

Blanch, J., Walter, T., Norman, L., Gunning, K., & de Groot, L. (2020). Solution separation-based FD to mitigate the effects of local threats on PPP integrity. In 2020 IEEE/ION Position, Location and Navigation Symposium (PLANS), IEEE, (pp. 1085–1092).

Blanch, J., Walker, T., Enge, P., Lee, Y., Pervan, B., Rippl, M., & Kropp, V. (2015). Baseline advanced RAIM user algorithm and possible improvements. *IEEE Transactions on Aerospace and Electronic Systems, 51*(1), 713–732.

Collins, P. (2008). Isolating and estimating undifferenced GPS integer ambiguities. In Proceedings of the 2008 National Technical Meeting of The Institute of Navigation (pp. 720–732).

Collins, P., Lahaye, F., Heroux, P., & Bisnath, S. (2008). Precise point positioning with ambiguity resolution using the decoupled clock model. In Proceedings of the

21st international technical meeting of the satellite division of the Institute of Navigation (ION GNSS 2008) (pp. 1315–1322).
DeCleene, B. (2006). Performance requirements for LPV approaches to minima as low as 200 ft above runway threshold. In International Civil Aviation Organization Navigation Systems Panel (NSP), Technical Working Group (WG1) Meeting.
El-Mowafy, A., & Kubo, N. (2020). Prediction of RTK positioning integrity for journey planning. *Journal of Applied Geodesy, 14*(4), 431–443.
Feng, S., Jokinen, A., Ochieng, W., Liu, J., & Zeng, Q. (2014). Receiver autonomous integrity monitoring for fixed ambiguity precise point positioning. *China Satellite Navigation Conference (CSNC) 2014 Proceedings* (Vol. II, pp. 159–169). Springer.
Gao, Y., Jiang, Y., Gao, Y., & Huang, G. (2021). A linear Kalman filter-based integrity monitoring considering colored measurement noise. *GPS Solutions, 25*(2), 1–13.
Ge, M., Gendt, G., Rothacher, M. A., Shi, C., & Liu, J. (2008). Resolution of GPS carrier-phase ambiguities in precise point positioning (PPP) with daily observations. *Journal of Geodesy, 82*(7), 389–399.
GEAS (2010) GNSS evolutionary architecture study, GEAS phase II panel report, FAA, Washington. Retrieved December 29, 2021, from https://www.gps.gov/cgsic/meetings/2010/eldredge2.pdf
Geng, J., & Guo, J. (2020). Beyond three frequencies: An extendable model for single-epoch decimeter-level point positioning by exploiting Galileo and BeiDou-3 signals. *Journal of Geodesy, 94*(1), 1–15.
Geng, J., Li, X., Zhao, Q., & Li, G. (2019). Inter-system PPP ambiguity resolution between GPS and BeiDou for rapid initialization. *Journal of Geodesy, 93*(3), 383–398.
Gunning, K., Blanch, J., Walter, T., de Groot, L., & Norman, L. (2018, September). Design and evaluation of integrity algorithms for PPP in kinematic applications. In Proceedings of the 31th International Technical Meeting of The Satellite Division of the Institute of Navigation (ION GNSS+ 2018).
Jokinen, A., Feng, S., Schuster, W., Ochieng, W., Yang, L., Moore, T., & Hill, C. (2013b, September). Improving ambiguity validation and integrity monitoring of Precise Point Positioning (PPP). In Proceedings of the 26th International Technical Meeting of the Satellite Division of the Institute of Navigation (ION GNSS+ 2013b) (pp. 1224–1233).
Jokinen, A., Feng, S., Schuster, W., Ochieng, W., Hide, C., Moore, T., & Hill, C. (2013a). Integrity monitoring of fixed ambiguity Precise Point Positioning (PPP) solutions. *Geo-Spatial Information Science, 16*(3), 141–148.
Laurichesse, D., & Banville, S. (2018). Innovation: Instantaneous centimeter-level multi-frequency precise point positioning. GPS World, 4.
Laurichesse, D., Mercier, F., Berthias, J. P., Broca, P., & Cerri, L. (2009). Integer ambiguity resolution on undifferenced GPS phase measurements and its application to PPP and satellite precise orbit determination. *Navigation, 56*(2), 135–149.
Li, T., Wang, J., & Laurichesse, D. (2014). Modeling and quality control for reliable precise point positioning integer ambiguity resolution with GNSS modernization. *GPS Solutions, 18*(3), 429–442.
Li, X., Huang, J., Li, X., Lyu, H., Wang, B., Xiong, Y., & Xie, W. (2021). Multi-constellation GNSS PPP instantaneous ambiguity resolution with precise atmospheric corrections augmentation. *GPS Solutions, 25*(3), 107.
Loyer, S., Perosanz, F., Mercier, F., Capdeville, H., & Marty, J. C. (2012). Zero-difference GPS ambiguity resolution at CNES–CLS IGS analysis center. *Journal of Geodesy, 86*(11), 991–1003.
Meng, Q., Liu, J., Zeng, Q., Feng, S., & Xu, R. (2019). Improved ARAIM fault modes determination scheme based on feedback structure with probability accumulation. *GPS Solutions, 23*(1), 1–11.
Racelis, D., & Joerger, M. (2020, September). Impact of Cascading Faults on Mega-Constellation-Augmented GNSS PPP Integrity. In Proceedings of the 33rd International Technical Meeting of the Satellite Division of The Institute of Navigation (ION GNSS+ 2020) (pp. 3055–3070).
Reid, T. G., Houts, S. E., Cammarata, R., Mills, G., Agarwal, S., Vora, A., & Pandey, G. (2019). Localization requirements for autonomous vehicles. arXiv preprint arXiv:1906.01061.
Richert, T., & El-Sheimy, N. (2007). Optimal linear combinations of triple frequency carrier phase data from future global navigation satellite systems. *GPS Solutions, 11*(1), 11–19.
Tao, J., Chen, G., Guo, J., Zhang, Q., Liu, S., & Zhao, Q. (2022). Toward BDS/Galileo/GPS/QZSS triple-frequency PPP instantaneous integer ambiguity resolutions without atmosphere corrections. *GPS Solutions, 26*(4), 1–14.
Wang, K., El-Mowafy, A., Qin, W., & Yang, X. (2022). Integrity monitoring of PPP-RTK positioning; Part I: GNSS-based IM procedure. *Remote Sensing, 14*(1), 44.
Wang, K., El-Mowafy, A., Rizos, C., & Wang, J. (2020). Integrity monitoring for horizontal RTK positioning: New weighting model and overbounding CDF in open-sky and suburban scenarios. *Remote Sensing, 12*(7), 1173.
Working Group C (2016) ARAIM Technical Subgroup Milestone 3 Report of the EU-US Cooperation on Satellite Navigation, Working Group C. Retrieved December 29, 2021, from https://www.gps.gov/policy/cooperation/europe/2016/working-group-c/.
Zhang, B., Chen, Y., & Yuan, Y. (2019). PPP-RTK based on undifferenced and uncombined observations: Theoretical and practical aspects. *Journal of Geodesy, 93*, 1011–1024.
Zhang, B., Teunissen, P. J., & Odijk, D. (2011). A novel un-differenced PPP-RTK concept. *The Journal of Navigation, 64*(S1), S180–S191.
Zhang, W., Wang, J., El-Mowafy, A., & Rizos, C. (2023). Integrity monitoring scheme for undifferenced and uncombined multi-frequency multi-constellation PPP-RTK. *GPS Solutions, 27*(2), 68. https://doi.org/10.1007/s10291-022-01391-4

Publisher's Note

Springer Nature remains neutral with regard to jurisdictional claims in published maps and institutional affiliations.

Submit your manuscript to a SpringerOpen journal and benefit from:

- ► Convenient online submission
- ► Rigorous peer review
- ► Open access: articles freely available online
- ► High visibility within the field
- ► Retaining the copyright to your article

Submit your next manuscript at ► springeropen.com